Volume-activated Chloride Permeability Can Mediate Cell Volume Regulation in a Mathematical Model of a Tight Epithelium

JON STRIETER, JOHN L. STEPHENSON, LAWRENCE G. PALMER, and ALAN M. WEINSTEIN

From the Department of Physiology and Biophysics, Cornell University Medical College, New York 10021

ABSTRACT Cell volume regulation during anisotonic challenge is investigated in a mathematical model of a tight epithelium. The epithelium is represented as compliant cellular and paracellular compartments bounded by mucosal and serosal bathing media. Model variables include the concentrations of Na, K, and Cl, hydrostatic pressure, and electrical potential, and the mass conservation equations have been formulated for both steady-state and time-dependent problems. Ionic conductance is represented by the Goldman constant field equation (Civan, M. M., and R. J. Bookman. 1982. *Journal of Membrane Biology.* 65:63–80). A basolateral cotransporter of Na, K, and Cl with 1:1:2 stoichiometry (Geck, P., and E. Heinz. 1980. *Annals of the New York Academy of Sciences.* 341:57–62.) and volume-activated basolateral ion permeabilities are incorporated in the model. MacRobbie and Ussing (1961. *Acta Physiologica Scandinavica.* 53:348–365.) reported that the cells of frog skin exhibit osmotic swelling followed by a volume regulatory decrease (VRD) when the serosal bath is diluted to half the initial osmolality. Similar regulation is achieved in the model epithelium when both a basolateral cotransporter and a volume-activated Cl permeation path are included. The observed transepithelial potential changes could only be simulated by allowing volume activation of the basolateral K permeation path. The fractional VRD, or shrinkage as percent of initial swelling, is examined as a function of the hypotonic challenge. The fractional VRD increases with increasing osmotic challenge, but eventually declines under the most severe circumstances. This analysis demonstrates that the VRD response depends on the presence of adequate intracellular chloride stores and the volume sensitivity of the chloride channel.

INTRODUCTION

The mechanisms by which cells maintain their volume in varying environments have been the subject of experimental investigation for nearly three decades. MacRobbie

Address reprint requests to Jon Strieter, Department of Physiology and Biophysics, Cornell University Medical College, 1300 York Avenue, New York, NY 10021.

This work was presented in part at the 73rd Annual Meeting of The Federation of American Societies of Experimental Biology in New Orleans, LA, 1989. (1989. *FASEB Journal.* 3:A1150).

and Ussing (1961) were the first to demonstrate volume regulation in the epithelial cells of frog skin. In isolated cells the avian red cell has served as a particularly useful model system for the study of cell volume regulation (Kregenow, 1981). When exposed to anisotonic media, duck erythrocytes exhibit osmometric swelling or shrinkage followed by a volume regulatory phase that restores their original cell volume (Kregenow, 1971*a*, *b*). In epithelial cells, volume homeostasis demands precise balance between apical and basolateral ion fluxes and water flow (Schultz, 1981). The toad urinary bladder and frog skin have served as the classic models of tight salt-transporting epithelia (Ussing and Zerahn, 1951; Koefoed-Johnsen and Ussing, 1958; Ussing and Windhager, 1964; Macknight et al., 1980). Although several mathematical models of these epithelia have been presented (Hviid Larsen, 1978; Lew et al., 1979; Civan and Bookman, 1982; Ferreira and Ferreira, 1983; Mintz et al., 1986) the model predictions of cell volume regulation have not been extensively investigated.

In this work, the Koefoed-Johnsen and Ussing (1958) picture of a transporting epithelium has been expanded to include a basolateral Na:K:Cl cotransporter and basolateral volume-dependent permeabilities for K and Cl. The existence of the triple cotransporter was first postulated by Geck and Heinz (1980) in Ehrlich ascites tumor cells. Important in epithelial chloride transport, Na:K:Cl cotransport has been identified in a large number of epithelia, including Amphiuma diluting segment (Oberleithner et al., 1983), mammalian thick ascending limb (Greger et al., 1983; Koenig et al., 1983), and rabbit renal papillary surface epithelium (Sands et al., 1986). Ferreira and Ferreira (1981) first suggested the coupling of basolateral ion fluxes in frog skin to explain epithelial cell volume regulation. Evidence supporting the existence of a basolateral Na:K:Cl cotransporter in frog skin has been offered by Ussing (1985). The presence of this cotransporter explains the high intracellular chloride concentration, which is well above its electrochemical equilibrium value in both frog skin (Rick et al., 1978*a*; Nagel et al., 1981; Giraldez and Ferreira, 1984) and toad bladder (Macknight et al., 1971; Rick et al., 1978*b*; Civan et al., 1980). Inclusion of the cotransporter alone, however, does not confer upon the model the ability to simulate cell volume regulation. The concept of a variable chloride permeability dependent on some intracellular parameter was first suggested by Hviid Larsen and Kristensen (1978) in toad skin. Further exploration of the original results of MacRobbie and Ussing (1961) prompted Ussing (1982) to propose that cell swelling induces an increase in the number of basolateral potassium and/or chloride channels in frog skin as well as activation of an electroneutral cotransport system. In toad bladder, Finn and Reuss (1975) likewise demonstrated a decrease in basolateral membrane resistance during exposure to a hypotonic serosal solution.

Increases in K and Cl permeabilities in response to cell swelling have been demonstrated in several nonpolar cells including Ehrlich ascites tumor cells (Hudson and Schultz, 1988; Hoffmann and Simonsen, 1989) and lymphocytes (Grinstein et al., 1984), as well as in several epithelia including *Necturus* small intestine (Lau et al., 1984), turtle colon (Germann et al., 1986), toad (Chase and Wong, 1985) and frog (Davis and Finn, 1987) urinary bladders, and proximal tubule (Kirk et al., 1987; Lopes and Guggino, 1987; Welling and Linshaw, 1988; Welling and O'Neil, 1990). Recently, Sackin (1989) has related membrane patch pressure manipulation to cell

volume changes, postulating a physiologic role for stretch-activation of K channels in proximal tubule cell volume regulation.

In this study we investigate the consequences of Ussing's hypothesis of volume-dependent permeabilities in a mathematical model of a tight epithelium. The basic model has been tailored to agree with that of Civan and Bookman (1982). In addition, we use a nonequilibrium thermodynamic description of Na:K:Cl cotransport due to Geck and Heinz (1980) and we formulate a three-parameter expression to describe the volume dependence of basolateral K and Cl permeabilities.

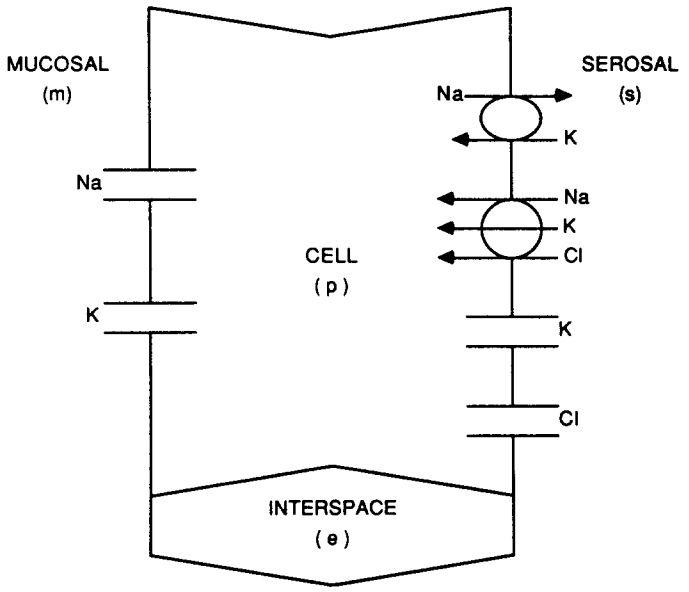

FIGURE 1. Schematic representation of toad bladder epithelial cell (p) with lateral intercellular space (e). Although all five membranes contain nonzero permeabilities for all three species, only the major conductances are shown. The basolateral membrane contains a metabolically driven Na/K exchanger, a Na:K:Cl cotransporter, and volume-activated K and Cl permeabilities.

MODEL EQUATIONS

The epithelium is represented as compliant cellular and paracellular compartments, bounded by well-stirred mucosal and serosal bathing media (Fig. 1). The system is thus composed of four compartments: mucosal solution (m), serosal solution (s), cellular compartment (p for principal cell), and lateral intercellular space (e). For each compartment, α, we consider the hydrostatic pressure, p^α, the electrical potential, ψ^α, and the electrolyte concentrations, C_k^α, where $k = 1, 2, 3$ denotes Na, K, and Cl, respectively. All activity coefficients are assumed to be unity. The volumes of the cell and interspace are denoted by V^p and V^e, respectively. In model simulations, pressure, electrical potential, and ionic concentrations within the cell and interspace are the system variables. To simulate experiments in an open-

circuited epithelium, the transepithelial potential is treated as a variable. Otherwise, mucosal and serosal bath concentrations, pressures, and potentials are given as boundary conditions.

There are five membranes in the system, subscripted according to the two compartments, α and β, that they separate: the apical membrane (mp), the basal cell membrane (ps), the lateral cell membrane (pe), the tight junction (me), and the interspace basement membrane (es). Across each membrane, $\alpha\beta$, there is a volume flow from compartment α to β, $J_v^{\alpha\beta}$, and for each species, k, a solute flux, $J_k^{\alpha\beta}$.

Mass conservation states that the volume loss from cell or interspace will be the net volume efflux:

$$-\frac{d}{dt}V^{\mathrm{p}} = J_v^{\mathrm{pe}} + J_v^{\mathrm{ps}} - J_v^{\mathrm{mp}} \tag{1}$$

$$-\frac{d}{dt}V^{\mathrm{e}} = J_v^{\mathrm{es}} - J_v^{\mathrm{pe}} - J_v^{\mathrm{me}}. \tag{2}$$

Likewise, solute loss from cell or interspace will be the net solute efflux:

$$-\frac{d}{dt}(C_k^{\mathrm{p}}V^{\mathrm{p}}) = J_k^{\mathrm{pe}} + J_k^{\mathrm{ps}} - J_k^{\mathrm{mp}}, \quad k = 1, 2, 3 \tag{3}$$

$$-\frac{d}{dt}(C_k^{\mathrm{e}}V^{\mathrm{e}}) = J_k^{\mathrm{es}} - J_k^{\mathrm{pe}} - J_k^{\mathrm{me}}, \quad k = 1, 2, 3. \tag{4}$$

Electroneutrality is preserved within cell and interspace throughout time according to

$$\sum_{k=1}^{3} z_k C_k^{\mathrm{p}} + z_{\mathrm{IMP}} C_{\mathrm{IMP}}^{\mathrm{p}} = 0 \tag{5}$$

and

$$\sum_{k=1}^{3} z_k C_k^{\mathrm{e}} = 0, \tag{6}$$

where z_k is the valence of species k, and z_{IMP} is the valence of the intracellular impermeant. In all, mass conservation and electroneutrality give a system of 10 equations in 10 unknowns.

To account for compartmental distention and shrinkage corresponding to fluctuations in pressure within the cell and interspace, compliance relations have been included. As in the *Necturus* gallbladder model of Weinstein and Stephenson (1979), the tight junctional area is assumed constant and the area of the interspace basement membrane, A^{es}, varies linearly with transmural pressure:

$$A^{\mathrm{es}} = A_0^{\mathrm{es}}[1 + \nu^{\mathrm{e}}(p^{\mathrm{e}} - p^{\mathrm{p}})]. \tag{7}$$

With essentially trapezoidal geometry, the interspace flares linearly to its widest area, $b \cdot A^{\mathrm{es}}$, at its midpoint and then tapers linearly to a fixed tight junctional area, A^{me}, so

that the volume of the interspace is

$$V^{e} = L(A^{es} + 2b \cdot A^{es} + A^{me})/4, \tag{8}$$

where L is the height of both the cell and the interspace, the equivalent of epithelial thickness. Similarly, the height of the cell is written as a linear function of intracellular pressure, in an effort to avoid large rises in hydrostatic pressure within the cell:

$$L = L_0[1 + \nu^{p}(p^{p} - p^{m})]. \tag{9}$$

This compliance relation adds an eleventh equation to the set of model equations for a total of eleven unknowns in the short-circuit configuration. The cell height is equivalent to epithelial volume (per square centimeter of epithelial area), so that the cell volume is the difference of epithelial volume and interspace volume:

$$V^{p} = L - V^{e}. \tag{10}$$

The volume flow across membrane $\alpha\beta$ is written

$$J_v^{\alpha\beta} = L_p^{\alpha\beta}\Delta p^{\alpha\beta} - L_p^{\alpha\beta}RT\sum_{k=1}^{3}\sigma_k^{\alpha\beta}\Delta C_k^{\alpha\beta}, \tag{11}$$

where $\Delta p^{\alpha\beta}$ and $\Delta C_k^{\alpha\beta}$ represent pressure and concentration differences, respectively, across the membrane $\alpha\beta$, $L_p^{\alpha\beta}$ is the water permeability, $\sigma_k^{\alpha\beta}$ is the reflection coefficient of species k, and RT is the product of gas constant and absolute temperature. Solute flux is the sum of convective, electrodiffusive, and active transport. As in previous models of frog skin and toad bladder (Hviid Larsen, 1978; Lew et al., 1979; Civan and Bookman, 1982) we used the Goldman constant field equation (1943) to describe electrodiffusive ionic fluxes. In this representation solute flux is given by

$$J_k^{\alpha\beta} = (1 - \sigma_k^{\alpha\beta})\overline{C}_k^{\alpha\beta}J_v^{\alpha\beta} + \frac{P_k^{\alpha\beta}z_kF\Delta\psi^{\alpha\beta}}{RT}\left[\frac{C_k^{\alpha} - C_k^{\beta}\exp\left(\frac{-z_kF\Delta\psi^{\alpha\beta}}{RT}\right)}{1 - \exp\left(\frac{-z_kF\Delta\psi^{\alpha\beta}}{RT}\right)}\right] + J_k^{act}, \tag{12}$$

where $\overline{C}_k^{\alpha\beta}$ is the mean membrane concentration of species k,

$$\overline{C}_k^{\alpha\beta} = \frac{\Delta C_k^{\alpha\beta}}{\Delta \ln C_k^{\alpha\beta}} = \frac{C_k^{\alpha} - C_k^{\beta}}{\ln (C_k^{\alpha}/C_k^{\beta})}, \tag{13}$$

$P_k^{\alpha\beta}$ is the permeability of membrane $\alpha\beta$ for species k, F is Faraday's constant, $\Delta\psi^{\alpha\beta}$ is the electrical potential difference across the membrane, and J_k^{act} is the active transport term.

A basolateral Na-K pump is included in the model. We employed the kinetic description of Hoffman and Tosteson (1971), also used in the models of Lew et al. (1979) and Civan and Bookman (1982). With three identical noncooperative sites for

Na and two for K, the pump flux for Na is written

$$J_{Na}^{act} = (J_{Na}^{act})_{max}\left[\frac{C_{Na}^{p}}{C_{Na}^{p} + K_{Na}}\right]^{3}\left[\frac{C_{K}^{s}}{C_{K}^{s} + K_{K}}\right]^{2}. \tag{14}$$

A stoichiometry of 3:2, as observed in frog skin by Nielsen (1979), gives the pump flux for K:

$$J_{K}^{act} = -\frac{2}{3}J_{Na}^{act}. \tag{15}$$

The variable affinities of the Na and K binding sites on the intracellular and serosal surfaces are represented according to Garay and Garrahan (1973):

$$K_{Na} = 0.2\left(1 + \frac{C_{K}^{p}}{8.33}\right) \tag{16}$$

$$K_{K} = 0.1\left(1 + \frac{C_{Na}^{s}}{18.5}\right). \tag{17}$$

The basolateral cotransporter of Na, K, and Cl with 1:1:2 stoichiometry is represented by the nonequilibrium thermodynamic description of Geck and Heinz (1980). Using the linear formalism, Geck and Heinz (1980) found tight coupling between furosemide-sensitive flows of Na, K, and Cl with a stoichiometry of 1:1:2 in Ehrlich ascites tumor cells. Writing the flux of the three species through the cotransporter as a vector in terms of the 3 × 3 matrix of Onsager coefficients, we have

$$\begin{bmatrix} J_{Na}^{cotr} \\ J_{K}^{cotr} \\ J_{Cl}^{cotr} \end{bmatrix} = L^{cotr}\begin{bmatrix} 1 & 1 & 2 \\ 1 & 1 & 2 \\ 2 & 2 & 4 \end{bmatrix}\begin{bmatrix} \Delta\bar{\mu}_{Na}^{\alpha\beta} \\ \Delta\bar{\mu}_{K}^{\alpha\beta} \\ \Delta\bar{\mu}_{Cl}^{\alpha\beta} \end{bmatrix}, \tag{18}$$

where $\alpha\beta$ is ps or pe for the basal or the lateral cell membrane, respectively, and the electrochemical potential is given by

$$\Delta\bar{\mu}_{k}^{\alpha\beta} = RT\Delta \ln C_{k}^{\alpha\beta} + z_{k}F\Delta\psi^{\alpha\beta}. \tag{19}$$

With this stoichiometry, the cotransporter is electroneutral, so that the potential terms in the electrochemical driving force sum to zero and cotransport is driven only by chemical gradients of the three ions (Geck et al., 1980). Although kinetic models of cotransporters exist (Turner, 1983), nonequilibrium thermodynamics requires minimal specification of cotransport parameters and the cotransport coefficient, L^{cotr}, is the only parameter that must be specified.

Ussing (1982) has proposed that cell swelling induces an elevation of the basolateral K and/or Cl permeability in frog skin. To investigate the role of these mechanisms in cell volume regulation, we have incorporated an expression for volume dependent permeability in the model. Basolateral permeability for ion k =

K, Cl is given by

$$P_k^{\alpha\beta} = P_k^0\left(1 + \frac{M_k}{1 + \exp\left(-\xi(V^p - V_{1/2}^p)\right)}\right), \tag{20}$$

where $\alpha\beta$ is ps or pe for the basal or lateral cell membrane, respectively, P^0 is the reference permeability, M_k is the maximum factor by which permeability may increase, $V_{1/2}^p$ is the cell volume at which the change in permeability is half of its maximum value, and ξ is the compliance of the basolateral channel. Fig. 2 shows the shape of the volume-activated Cl permeability for $M_{Cl} = 100$, $\xi = 5 \times 10^5\ cm^{-1}$, and $V_{1/2}^p = 1.8 \times 10^{-3}\ cm^3/cm^2$. A similar expression has been used by Huss and Marsh (1975) to describe channel compliance in their model of the paracellular pathway of the proximal tubule epithelium.

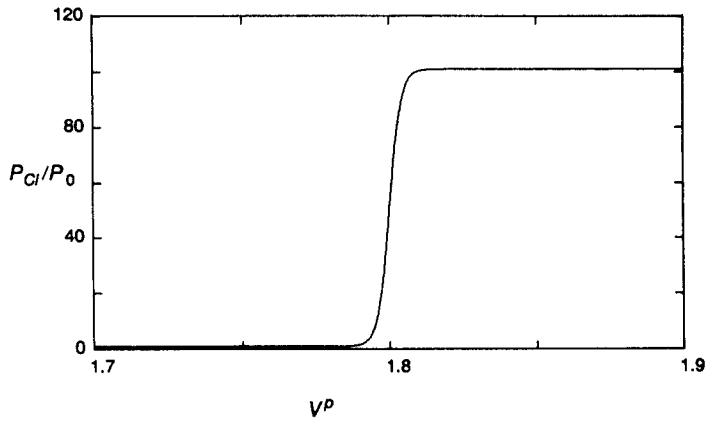

FIGURE 2. Graph of volume-dependent chloride permeability function, P_{Cl}, as a function of cell volume V^p ($10^{-3}\ cm^3/cm^2$), with $M_{Cl} = 100$, $V_{1/2}^p = 1.8 \times 10^{-3}\ cm^3/cm^2$, and $\xi = 5 \times 10^5\ cm^{-1}$.

CHOICE OF PARAMETERS AND NUMERICAL SOLUTION

Previous models of toad bladder and frog skin have provided a basic set of parameters, which we have expanded to investigate cell volume regulation. A complete list of parameters appears in Table I. Values were chosen so that the steady-state short-circuit simulation with zero basolateral cotransport agrees with that of Civan and Bookman (1982). Lew et al. (1979) and Civan and Bookman (1982) offer detailed discussion of this set of parameters in their presentations.

In contrast to the previous models, our formulation requires the quantitative specification of epithelial geometry and individual membrane water permeabilities. DiBona (1978) determined that granular cells comprise 96.5% of the apical surface area of the Dominican toad bladder epithelium with a total perimeter of 1,431 cm/cm^2. The toad urinary bladder has a low water permeability in the absence of ADH (Hays and Leaf, 1962). Under basal conditions, the apical membrane constitutes the rate-limiting barrier to transepithelial water flow. The apical water perme-

ability has been chosen consistent with the water flow measurements of Hays and Leaf (1962) for unstimulated toad bladder. Measurements of ADH-stimulated bladders provide a lower limit for the basolateral water permeability. Consistent with the observation that whole epithelial water permeability can increase 100-fold with ADH stimulation (Levine et al., 1984), the basolateral permeability has been chosen to be approximately two orders of magnitude greater than the apical. The paracellular pathway has traditionally been considered a physiologically insignificant route for water transport in tight epithelia. Because experimental determinations of tight

TABLE I

Parameter Values

Dimensions and impermeant species concentrations				
Cell height (L), *cm*			$L = 0.001[1 + 0.8(p^{p} - p^{m})]$	
Interspace basement membrane area (A^{cs}), *cm²/cm² epithelium*			$A^{cs} = 0.011[1 + 0.13(p^{c} - p^{p})]$	
Interspace volume (V^{c}), *cm³/cm² epithelium*			$V^{c} = L[A^{mc} + 20 \cdot A^{cs} + A^{cs}]/4$	
Reference cell volume (V_0^{p})			1.74×10^{-3} cm³/cm² epithelium	
Reference impermeant species concentration ($C_{IMP,0}$)			46.2 mM	
Actual impermeant species concentration			$C_{IMP} = C_{IMP,0}(V_0^{p}/V^{p})$	
Membrane properties				
Tight junction		Interspace basement membrane	Apical membrane	Basolateral membrane
Water permeability, L_p(*cm³/s·mmHg·cm² epithelium*)				
6×10^{-10}		3×10^{-6}	6×10^{-10}	7×10^{-8}
Reflection coefficients, σ				
Na	1.0	0.0	1.0	1.0
K	1.0	0.0	1.0	1.0
Cl	1.0	0.0	1.0	1.0
Goldman permeabilities, P_k(*cm³/s·cm² epithelium*)				
Na	5.0×10^{-8}	1.3×10^{-2}	6.5×10^{-7}	7.3×10^{-8}
K	7.0×10^{-8}	1.3×10^{-2}	1.0×10^{-7}	1.8×10^{-5}
Cl	2.5×10^{-8}	1.3×10^{-2}	1.9×10^{-8}	1.8×10^{-7}
Na:K:Cl cotransport coefficient (*mmol²/J·s·cm² epithelium*)				
L^{cotr}				2.4×10^{-8}

junctional water permeability are lacking, we have set this parameter equal to its value for the unstimulated apical membrane. Again for lack of experimental data, the interspace basement membrane water permeabilities were chosen sufficiently large to give equal serosal and interspace ionic concentrations under all conditions.

The numerical methods used here have been used previously in the solution of models of the urinary concentrating mechanism (Stephenson, 1978) as well as in epithelial models (Weinstein and Stephenson, 1979). Denoting the vector of intracellular and interspace pressures, potentials, concentrations, and cell height for the

nth time step as γ^n and the system of equations as ϕ, we seek a solution γ^{n+1} to

$$\phi(\gamma^{n+1}, \gamma^n) = 0,$$

where γ^n is either known as a set of initial steady-state values, or is from a previous time step. Note that γ^n is an 11-vector in the short-circuit configuration and a 12-vector in the open-circuit configuration, with the addition of mucosal potential as a variable. In the solution of time-dependent problems, the above system of equations is replaced by finite difference equations centered in time. The resulting nonlinear equations are then solved iteratively using Newton's method, so that an

TABLE II

Solution of the Model Equations for the Open-Circuited Epithelium between Equal Ringer's Solutions

		V^c	V^p		
		$10^{-3}cm^3/cm^2$			
		0.09	1.74		
	ψ^m	ψ^c	ψ^p	ψ^s	
		mV			
	−68.2	0.0	−87.3	0.0	
	p^m	p^c	p^p	p^s	
		$mmHg$			
	0.0	0.0	1.0	0.0	
	C_k^m	C_k^c	C_k^p	C_k^s	
		mM			
Na	120.0	120.0	7.8	120.0	
K	2.5	2.5	134.3	2.5	
Cl	122.5	122.5	56.6	122.5	
IMP			46.2		
	J_k^{mc}	J_k^{mp}	J_k^{pc}	J_k^{cs}	J_k^{ps}
			$pmol/s \cdot cm^2$		
Na	−16.2	108.0	63.6	47.4	44.4
K	−0.5	−8.6	−5.1	−5.6	−3.6
Cl	82.6	0.3	0.2	82.7	0.1

initial guess γ_0^{n+1} is improved by applying Gaussian elimination to the linear system

$$G \cdot \Delta\gamma_0^{n+1} = \phi(\gamma_0^{n+1}, \gamma^n)$$

to compute the correction vector $\Delta\gamma_0^{n+1}$, where G is the approximate Jacobian matrix obtained by numerical differentiation, $\partial\phi/\partial\gamma$, evaluated at γ_0^n. The model was coded in FORTRAN and calculations were done on an HP 9000, model 540.

RESULTS

Table II displays the solution to the open-circuited epithelium in isotonic bathing media with inclusion of the cotransporter. The cotransporter accounts for elevation

of the intracellular chloride concentration to 57 mM from its equilibrium value of 5 mM. In this reference state, the flux of Na into the cell through the cotransporter is 16.9 pmol/s·cm^2, or 10.8% of the Na pump flux. Thus, although the cotransporter is operative, there is relatively little net flux through it because it is operating near the chemical equilibrium. In other words, to achieve a satisfactory cell Cl concentration, L^{cotr} must be nonzero although the cotransporter may be poised near equilibrium with little flux through it.

Upon reducing the osmolality of the serosal medium bathing frog skin to one-half its original value, MacRobbie and Ussing (1961, see Fig. 4) observed that the epithelial cells swell to a peak volume and subsequently shrink to a new steady-state volume. This shrinkage has been termed volume regulatory decrease (VRD). Upon restoration of full-strength Ringer, the cells initially shrink to a trough volume and subsequently swell to approach their original steady-state volume, thereby exhibiting a volume regulatory increase (VRI). MacRobbie and Ussing (1961) showed that KCl is lost during VRD and gained during VRI. Fig. 3 displays the time course of cell volume in a model simulation of the MacRobbie and Ussing experiment without the inclusion of volume-activated basolateral permeabilities. The initial state of the epithelium corresponds to the solution in Table II, so that the epithelium is open-circuited with 120 mM NaCl and 2.5 mM KCl bathing both sides. At 5 min the serosal bath osmolality is reduced to half-strength Ringer's. Cell volume rises rapidly during the first minute after hypotonic shock and then continues to increase only minimally. At 15 min the serosal bath is restored to full strength and cell volume returns to its original steady-state value. Thus, without inclusion of the volume-dependent permeabilities, the cell simply behaves as an osmometer.

Fig. 4 displays the effects of introducing a volume-activated basolateral K permeability. The volume response is nearly identical to the case without variable permeability, so that activation of the K permeability alone is incapable of inducing volume regulation. The response of the transepithelial potential is quite different. During the hypotonic phase, the rise in basolateral K permeability causes a hyperpolarization of the potential. The initial part of the restoration phase shows a triphasic response which is best understood by examining the changes in basolateral membrane potential. Initially, a transient depolarization is seen which results from the increase in serosal K concentration. The subsequent exit of water from the cell causes a concentration of intracellular K with a resultant hyperpolarization. Finally, the third phase corresponds to the decrease in K permeability upon cell shrinkage with consequent return to the steady-state potential.

The response to hypotonic shock in a cell with volume-activated basolateral Cl permeability alone is shown in Fig. 5. Cell volume increases to a peak within 1 min and then relaxes to a new steady-state within 10 min, exhibiting a VRD. As the serosal bath is restored to full strength, the cells shrink initially and subsequently exhibit a VRI. In this simulation, the chloride channel parameters are as in Fig. 2. Thus, volume activation of the basolateral chloride permeability is sufficient to simulate cell volume regulation. Although both VRD and VRI are clearly simulated with this model, differences between experimental and model time courses remain. Experimental volume changes take longer than those predicted by the model. Specifically, MacRobbie and Ussing found a time to peak volume of 5–13 min,

compared with 1 min for the model. This discrepancy may reflect the presence of unstirred layers (~0.5–1 mm) in the experimental preparation delaying the penetration of the hypotonic solution to the membrane surface. Times for relaxation to steady state, however, are comparable. The greatest discrepancy between model and experiment resides in the transepithelial potential. The simulated transepithelial potential reproduces neither the hyperpolarization during VRD nor the transient depolarization at the beginning of the restoration phase.

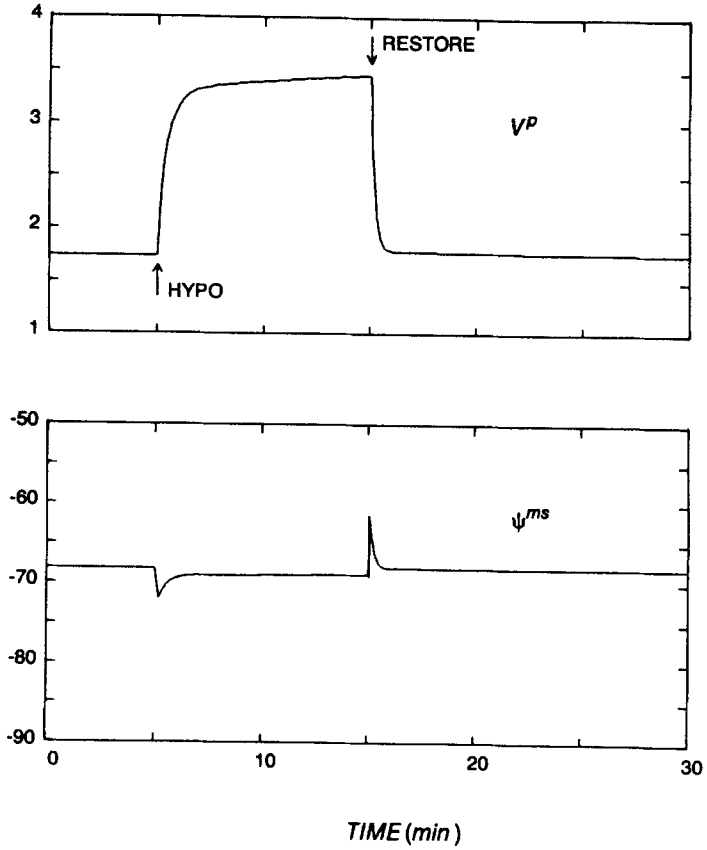

FIGURE 3. Model simulation of serosal hypotonic shock and restoration experiment demonstrating osmometric behavior without inclusion of volume-activated permeabilities. At $t = 5$ min the serosal bath is diluted to one-half its initial osmolality (HYPO). At $t = 15$ min the serosal bath is restored to full-strength Ringer's (RESTORE). The time courses of cell volume, V^P (10^{-3} cm^3/cm^2), and transepithelial potential, ψ^{ms} (millivolts), are shown.

The discrepancies in the simulation of transepithelial potential can be resolved by including volume-activated basolateral permeabilities for both K and Cl as shown in Fig. 6. The increase in K permeability after hypotonic shock induces the hyperpolarization during VRD. Upon restoration, the transient depolarization and subsequent repolarization are consequences of serosal, followed by intracellular increases in K

concentration (as in Fig. 5). Thus, it is the volume-activated Cl permeability that bestows volume regulation on the cell, although it is the volume-activated K permeability that permits reproduction of the experimental changes in transepithelial potential. Although the simulated repolarization is faster than that observed, the major remaining discrepancy is the gradual hyperpolarization during VRI found experimentally. This may, in fact, be simulated by altering the parameters of the

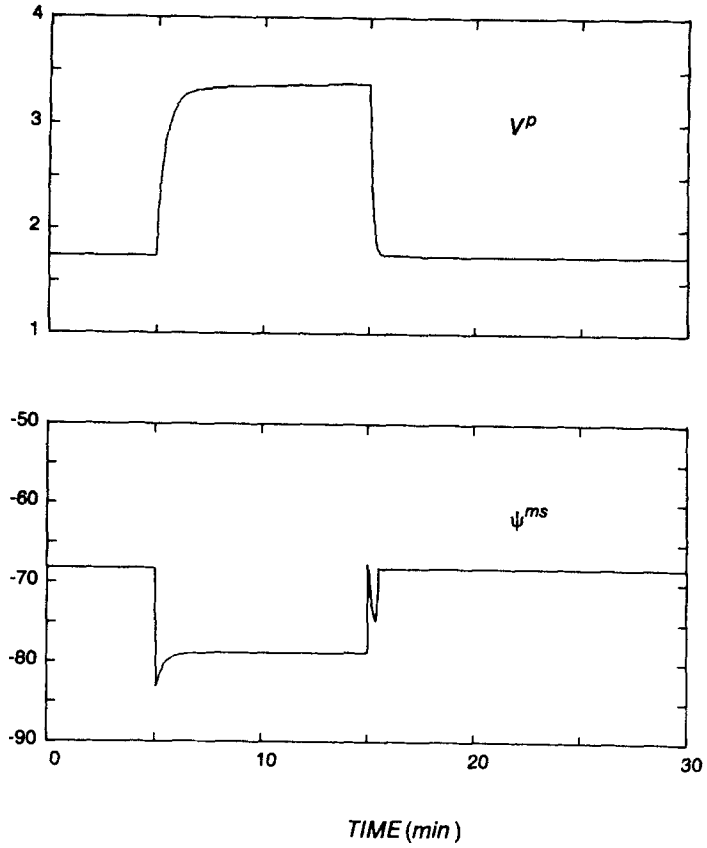

FIGURE 4. Model simulation of hypotonic shock experiment including volume-activated basolateral K permeability only, with $M_K = 10$, $V^p_{1/2} = 1.8 \times 10^{-3}$ cm, and $\xi = 5 \times 10^5$ cm^{-1}. Cell volume, V^p (10^{-3} cm^3/cm^2), and transepithelial potential, ψ^{ms} (millivolts), are shown.

volume-activated function for K permeability during the restoration phase, thus decreasing the K permeability below the steady-state value in response to cell shrinkage. Lewis et al. (1985) and Macknight (1985) have provided experimental evidence that shrinkage of toad bladder epithelial cells can result in a reduction of the number of basolateral K channels. However, justifying the incorporation of different permeability expressions for K and Cl into the model requires further

experimental examination of the volume-sensitive behavior of both of these channels.

To understand the volume regulation produced by the volume-activated Cl permeability, we investigated the responses of the cellular variables. Fig. 7 shows the

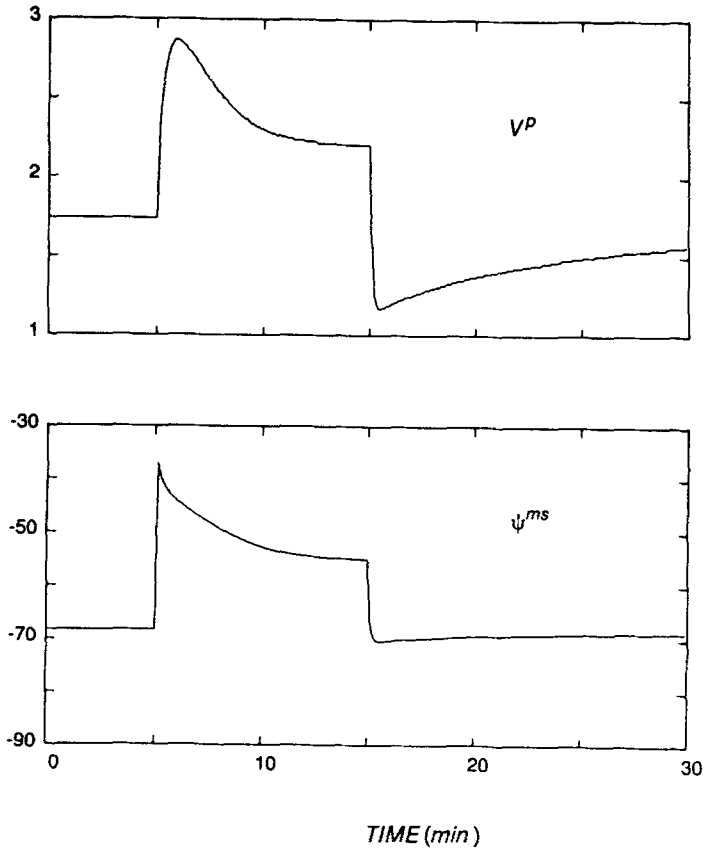

FIGURE 5. Model simulation of hypotonic shock experiment including volume-activated basolateral Cl permeability only, with $M_{Cl} = 100$, $V^p_{1/2} = 1.8 \times 10^{-3}$ cm, and $\xi = 5 \times 10^5$ cm^{-1}. Upon serosal bath dilution, cell volume V^p (10^{-3} cm^3/cm^2) initially rises, but subsequently declines exhibiting a VRD. As the serosal bath is restored to full strength, the cells initially shrink, yet subsequently swell exhibiting a VRI. Transepithelial potential, ψ^{ms} (millivolts), is also shown. Although cell volume regulation is demonstrated, the experimentally observed potential is not reproduced.

time course of intracellular ionic concentrations and cell potential for the simulation of Fig. 5. Volume fluctuations merely act to dilute or concentrate the initial cell sodium. In contrast, although initially diluted by cell swelling, KCl leaves the cell during VRD (Cl concentration decreases and K concentration remains the same as cell volume decreases). The volume-activated increase in basolateral chloride permeability causes a depolarization of the cell as shown. However, subsequent decreases

in cell Cl cause a repolarizing effect during VRD. These changes in cell potential are absent if the volume dependence is removed. Thus, if the chloride permeability were activated by depolarization as opposed to swelling, regulation could not be achieved. This argues against voltage-gated chloride channels as a mechanism of volume regulation in this epithelium. Fig. 8 shows the time course of intracellular ionic concentrations and cell potential for the simulation of Fig. 6, in which both

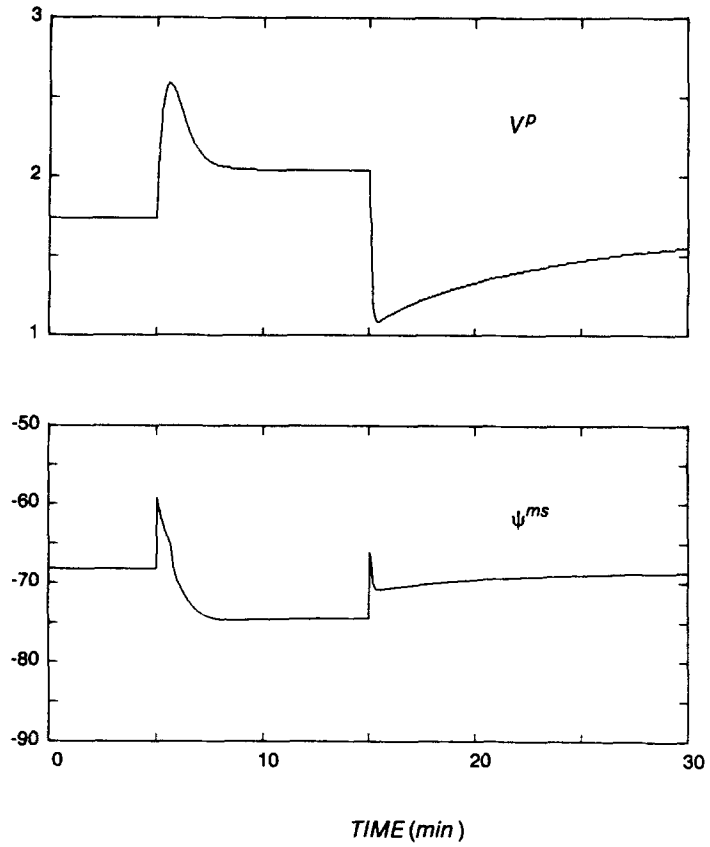

FIGURE 6. Model simulation of hypotonic shock experiment including volume-activated basolateral permeabilities for both K and Cl. Parameters for the permeability expressions are as in Figs. 4 and 5. Cell volume, V^P (10^{-3} cm^3/cm^2), and transepithelial potential, ψ^{ms} (millivolts), are shown. Cell volume regulation is demonstrated and the observed potential is reproduced.

volume-activated K and Cl permeabilities are included. The intracellular concentrations are qualitatively similar to those of Fig. 7, although cell Na concentration rises above the initial steady state during VRD as a consequence of cell hyperpolarization. The volume-activated increase in basolateral K permeability reduces the magnitude of the initial depolarization prior to VRD and subsequently causes a hyperpolarization of the basolateral membrane which is maintained throughout VRD. The

decrease in this permeability during VRI results in the return to the steady-state cell potential. In general, inclusion of the volume-activated K permeability stabilizes the overall changes in cell potential (as compared with Fig. 7). Additionally, by including the volume-activated K permeability, the changes in cell potential are reflected in the transepithelial potential, which more closely simulates the result of MacRobbie and Ussing. Comparison of Figs. 7 and 8 shows that by measuring cell potential, the presence of a volume-activated Cl permeability alone or volume-activated K and Cl permeabilities should be distinguishable experimentally.

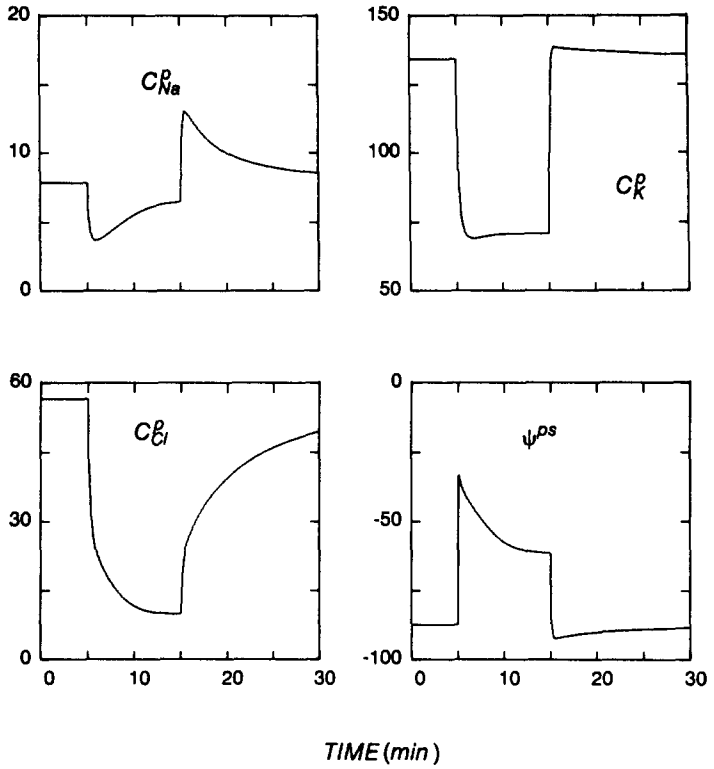

FIGURE 7. Time course of intracellular variables during simulation of experiment of Fig. 5 (with volume-activated Cl permeability only). Intracellular concentrations (millimolar) of the three ionic species as well as cell potential (millivolts) relative to the serosal bath are shown.

Fig. 9 graphically dissects the two components of basolateral chloride transport, channel flux and cotransport flux, for the simulation of Fig. 5. In the initial steady state, cotransport flux is directed into the cell accounting for the high cell Cl concentration. Coinciding with serosal bath dilution, the flux through the cotransporter increases substantially and changes direction. This phenomenon results from the sudden change in chemical gradients caused by serosal dilution, which precedes intracellular dilution. As soon as water flow into the cell induces intracellular dilution of all three species, the chemical gradient for inwardly directed cotransport becomes

significant. The cotransporter therefore tends to increase cell volume during the VRD. The Na:K:Cl cotransport is incapable of generating a VRD without the support of other regulatory mechanisms. Within the framework of this model, it is the coupling of the volume-activated chloride permeability with Na:K:Cl cotransport that permits volume regulation. After cell swelling, flux through the basolateral Cl channel is markedly increased as a result of the elevated Cl permeability. This exit of Cl through the channel with accompanying exit of K through its channel accounts for the observed VRD. As seen in Fig. 5, to generate a VRD, outwardly directed

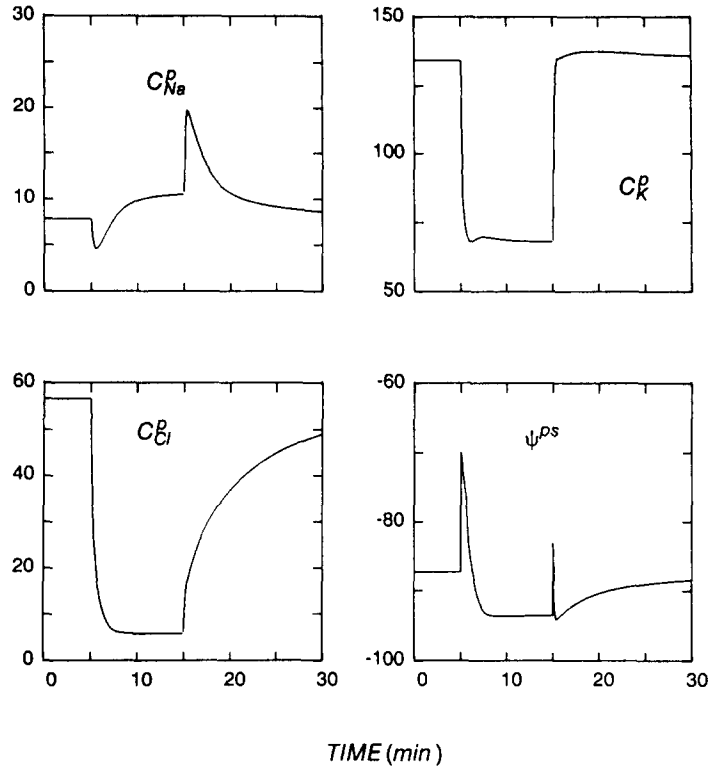

FIGURE 8. Time course of intracellular variables during simulation of experiment of Fig. 6 (with volume-activated K and Cl permeabilities). Intracellular concentrations (millimolar) of the three ionic species as well as cell potential (millivolts) relative to the serosal bath are shown.

(positive) channel flux must surpass inwardly directed (negative) cotransport flux after cell swelling. Upon restoration of full-strength Ringer, cell shrinkage causes a return of the chloride permeability to its baseline value with consequent reduction of Cl exit. However, Cl continues to enter the cell via the cotransporter now surpassing the opposing channel flux. This net entry of KCl accounts for the VRI. As cell shrinkage concentrates the intracellular ions, the inwardly directed chemical gradient for cotransport is reduced so that cotransport flux diminishes to its originally low value as cell volume recovers.

Fig. 10 shows that KCl movement may be limited by lowering the resting basolateral K permeability. The simulation is the same as in Fig. 5, although the fixed K permeability is one-tenth the value of that in Fig. 5, so that the initial cell volume is increased and extrusion of KCl during VRD is markedly reduced, effectively blocking volume regulation. This theoretical prediction is confirmed by the experimental result of Davis and Finn (1987), who eliminated volume regulation in frog urinary bladder upon application of barium.

Because the precise nature of volume activation of the chloride permeability is unclear, we investigated the effect of changes in the parameters defining the permeability expression as well as changes in the degree of hypotonic shock, on the

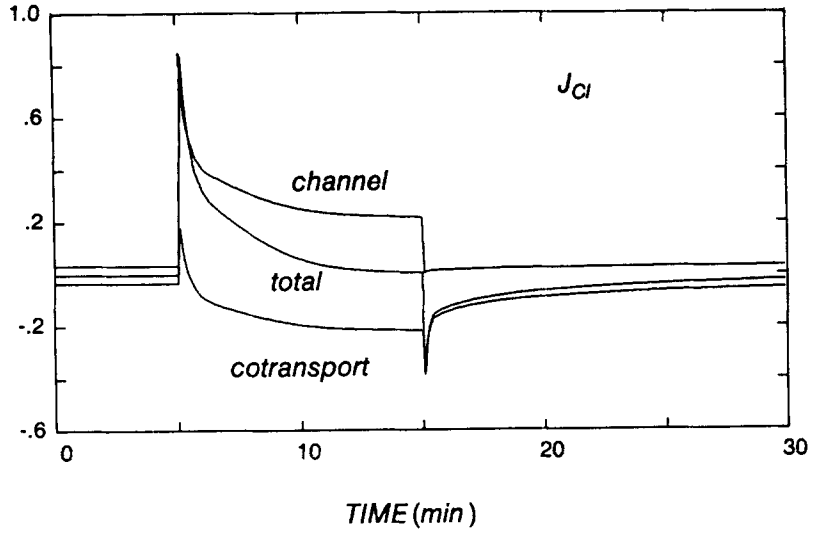

FIGURE 9. Time course of basolateral chloride fluxes in the experiment of Fig. 5. J_{Cl} (nanomoles/s·cm^2) is positive for fluxes directed from the cell towards the serosal bath. Flux through the basolateral chloride channel (channel), flux through the triple cotransporter (cotransport), and the sum of these two (total) are shown.

extent of VRD achieved in the model. To this end, we define the fractional volume regulatory decrease FVRD as follows:

$$FVRD = \frac{(V^p_{peak} - V^p_{hypo})}{(V^p_{peak} - V^p_{ref})},$$

where V^p_{ref} is the reference volume corresponding to the solution of Table II (full-strength Ringer's), V^p_{hypo} is the steady-state cell volume in a hypotonic serosal bath, and V^p_{peak} is the peak cell volume or overshoot before the VRD. FVRD = 1 for full recovery to the reference volume and FVRD = 0 for an osmometer. For Fig. 5, FVRD = 0.59. This compares favorably with MacRobbie and Ussing's values of 0.19–0.70 (1961, see Table IV).

Fig. 11 *a* analyzes the relationship between FVRD and $V^{p}_{1/2}$ (the volume at which the electrodiffusive chloride permeability is approximately half of its maximum value), with M_{Cl} (the maximum factor by which the Cl permeability may increase) = 100 and the channel compliance $\xi = 5 \times 10^5$. The curve plots the data from eight hypotonic shock simulations of the same nature as in Fig. 5 (serosal Ringer reduced to half strength). As $V^{p}_{1/2}$ increases up to 2.2×10^{-3} cm^3/cm^2, FVRD shows little

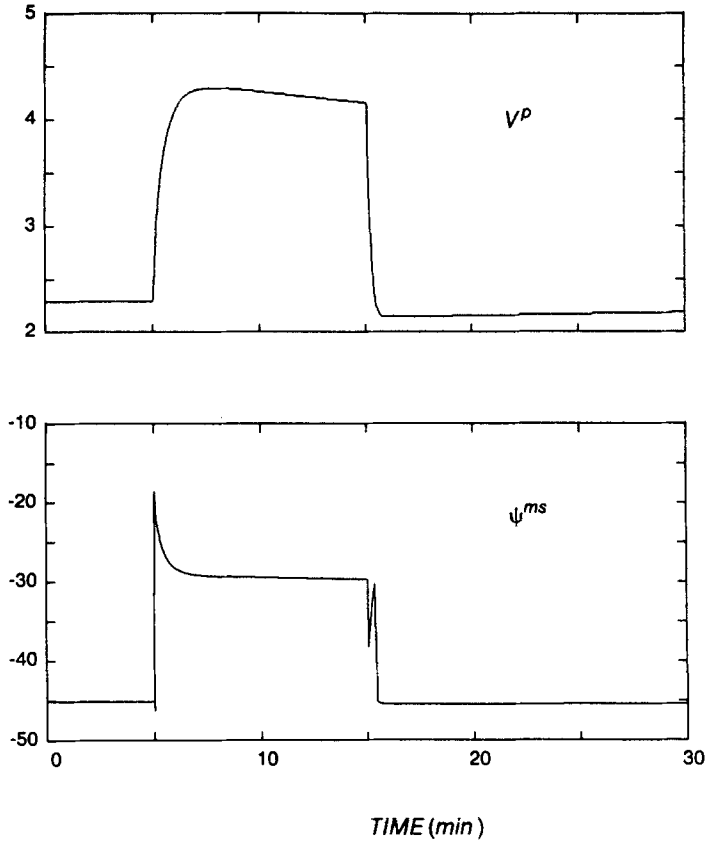

FIGURE 10. Model simulation of hypotonic shock experiment with reduced basolateral K permeability, including volume-activated basolateral Cl permeability only, with $M_{Cl} = 100$, $V^{p}_{1/2} = 2.4 \times 10^{-3}$ cm, and $\xi = 5 \times 10^5$ cm^{-1}. Initial cell volume is increased and volume regulation is virtually eliminated.

change. Beyond 2.2×10^{-3} cm^3/cm^2, however, FVRD decreases monotonically. With increasing values of $V^{p}_{1/2}$, the initial amount of swelling as well as the final steady-state volume V^{p}_{hypo} increase, so that FVRD must decrease.

The effect of changing the parameter M_{Cl} on FVRD is explored in Fig. 11 *b*, where FVRD is a function of M_{Cl}, with $V^{p}_{1/2} = 1.80$ and $\xi = 5 \times 10^5$. Again, the results of nine simulations are plotted to generate the curve. FVRD saturates at $M_{Cl} \approx 100$.

This reflects the finite amount of chloride within the cell that can exit through its channel during VRD. In physiological terms, the steady-state volume in hypotonic bath or V^p_{hypo} is determined by a balance between the leak chloride permeability and the cotransport coefficient. Once the permeability is raised high enough, the steady-state intracellular chloride cannot fall further.

Although not shown, the slope of the volume-activated permeability function, ξ, also affects the degree of volume regulation. While a 10-fold decrease in the slope

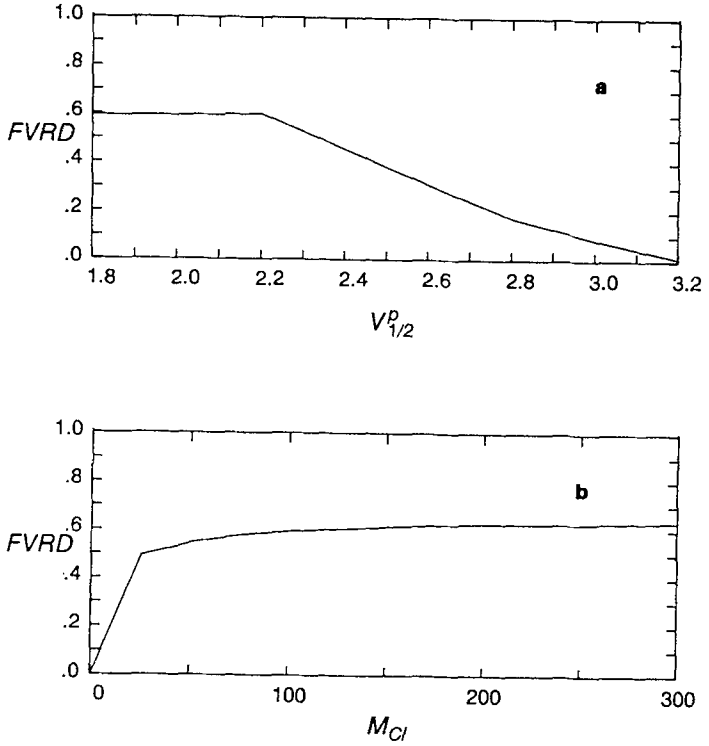

FIGURE 11. *a*, FVRD as a function of $V^p_{1/2}$ (10^{-3} cm^3/cm^2). The results of eight simulations were plotted to generate the curve shown. *b*, FVRD as a function of M_{Cl}. The results of nine simulations were plotted to generate the curve shown.

gives an effectively indistinguishable result, further reduction generates much less impressive volume regulation. In addition, to achieve comparable simulations with equivalent initial cell volumes, alteration of the slope requires alteration of M and $V^p_{1/2}$ as well.

Fig. 12 *a* shows the effect of varying degrees of hypotonic shock on FVRD, with $V^p_{1/2} = 1.80$, $M_{Cl} = 100$, and $\xi = 5 \times 10^5$. The results of eight model simulations are plotted. FVRD exhibits a peak and subsequent decline. To understand this relationship, Fig. 12 *b* shows the numerator, $V^p_{peak} - V^p_{hypo}$, and the denominator, $V^p_{peak} - V^p_{ref}$, of the expression for FVRD. As expected, the initial swelling, $V^p_{peak} -$

V^p_{ref}, increases steadily with increasing hypotonic challenge. In contrast, the absolute VRD, $V^p_{peak} - V^p_{hypo}$, reaches a maximum value and then decreases. The absolute VRD reflects the difference between the amount of cell chloride at peak and at the final steady state. As shown in Fig. 12 *c*, greater hypotonic shock diminishes the cell chloride concentration at peak volume (peak C^p_{Cl}). The final steady-state chloride concentration (hypo C^p_{Cl}), however, decreases initially and then levels off. Since the

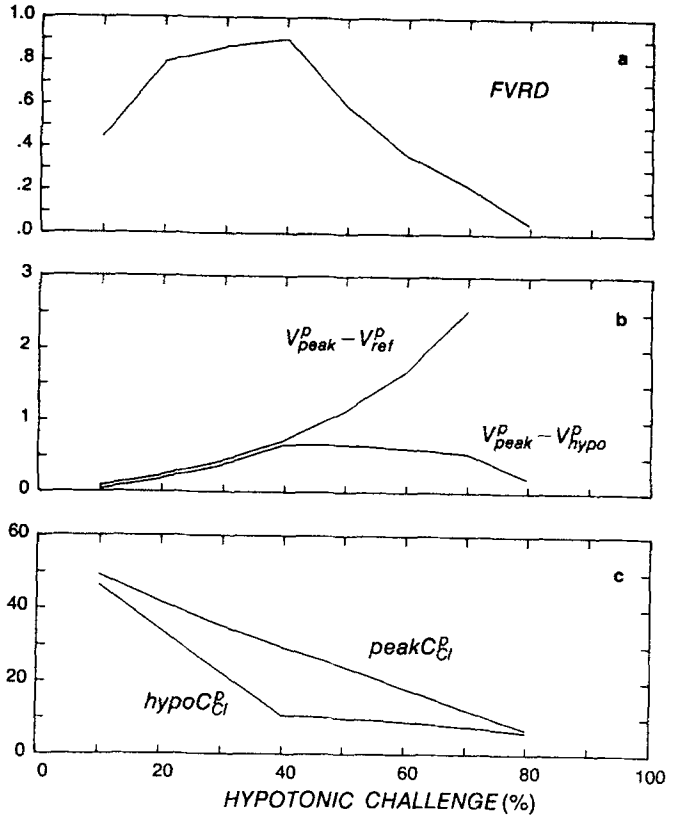

FIGURE 12. *a*, FVRD as a function of hypotonic challenge (hypotonic bath osmolality/reference osmolality). The results of eight simulations were plotted to generate the curve shown. *b*, $V^P_{peak} - V^P_{ref}$ and $V^P_{peak} - V^P_{hypo}$ (10^{-3} cm^3/cm^2) as a function of hypotonic challenge. *c*, Intracellular chloride concentration at peak volume (peak C^p_{Cl}) and at final steady-state volume (hypo C^p_{Cl}) as a function of hypotonic challenge.

steady-state chloride concentration is critically dependent on the chloride channel permeability, this may be understood by noting that the steady-state permeability increases and then levels off as well (see Fig. 2). Thus, as final and peak chloride concentrations initially diverge and then converge, FVRD initially increases and then declines.

DISCUSSION

Toad urinary bladder and frog skin have traditionally been studied as classic tight salt-transporting epithelia (Koefoed-Johnsen and Ussing, 1958; Macknight et al., 1980). They are particularly convenient to model because of their relative homogeneity of cell type and the secure view of salt transport in the predominant granular cell. Modeling studies of cell volume regulation in these epithelia have centered on the response to increases in apical Na entry. A relation describing the downregulation of apical Na permeability by mucosal and intracellular Na concentrations has been included in the more recent mathematical models (Civan and Bookman, 1982; Ferreira and Ferreira, 1983; Mintz et al., 1986). Incorporation of this concentration-dependent Na permeability permits the maintenance of steady-state cell volume in the face of increasing pump inhibition. Other regulatory mechanisms have received little attention in the modeling literature. The hypothesized coupling between apical and basolateral conductances was briefly investigated in a steady-state simulation (Hviid Larsen, 1978). By maintaining a constant ratio of apical Na permeability to basolateral K permeability, cell volume remained relatively constant despite increases in short-circuit current. Indeed, Davis and Finn (1982) have demonstrated a reduction in basolateral K conductance after inhibition of apical Na permeability. Similar regulation of steady-state cell volume under increases in short-circuit current was demonstrated in a mathematical model by Strieter et al. (1987) via the inclusion of a Na:K:Cl cotransporter, although an increase in the number of basolateral sodium pumps provided regulation as well.

This work has concentrated on modeling the capacity of ion transport mechanisms in the basolateral membrane to regulate cell volume in the granular cell during hypotonic challenge. The original model of Lew et al. (1979) has been extended with the addition of a basolateral electroneutral Na:K:Cl cotransporter and basolateral volume-activated K and Cl permeabilities. The volume-activated permeabilities together with the cell compliance relation represent the first incorporation of compliant channels into a model of epithelial transport. The triple cotransporter elevates steady-state intracellular chloride concentration to a value above equilibrium, in accordance with experimental data. Inclusion of the volume-activated chloride permeability and cell compliance relation bestows volume regulatory capacity on the model, particularly the ability to simulate VRD in response to hypotonic challenge. Furthermore, inclusion of a volume-activated basolateral K permeability is necessary to reproduce the transepithelial potential results of MacRobbie and Ussing. These modeling results support Ussing's hypothesis (1982): (*a*) a basolateral Na:K:Cl cotransporter raises steady-state intracellular chloride in frog skin epithelial cells; (*b*) exposure to serosal hypotonicity causes an initial cell swelling, which induces an increase in basolateral KCl permeability, allowing the extrusion of KCl and generating a VRD; and (*c*) upon restoration of isotonicity, the inwardly directed cotransport of solute generates a VRI. Further, the model predicts different roles for K and Cl. Specifically, K influences the behavior of transepithelial and cell potential, whereas Cl determines the volume regulatory capacity of the cell.

In considering volume-activated channels, we have attempted to test, in an epithelial model, the viability of Ussing's hypothesis of cell volume regulation in frog

skin. Further experimental data are required before the volume-dependent nature of the basolateral permeabilities can be definitively formulated in a mathematical model. The permeability expression used in this model assumes a steplike saturable activation of the channel. It is phenomenological in that intervening processes are neglected. Most directly, basolateral K (Sackin, 1987) and Cl (Ubl et al., 1988) channels could be activated by mechanical stress on the membrane as a result of the swelling. Alternatively, calcium could act as a second messenger in the signal transduction process. Calcium-activated conductive pathways for both K and Cl have been found in turtle colon (Chang and Dawson, 1988) and Ehrlich cells (Hoffmann et al., 1986). Wong and Chase (1986) have demonstrated that cell swelling increases intracellular calcium and that extracellular calcium is necessary for volume regulation in toad bladder epithelial cells. Other volume-sensitive intracellular parameters could also be the direct activator of the channel. Cala (1980) has suggested that the fluxes responsible for volume regulation in Amphiuma erythrocytes are activated by changes in intracellular pH, which is associated itself with osmotic changes. It is not clear, however, whether the pH changes are primary or secondary in relation to the permeability changes. Clearly, chloride-bicarbonate exchange or any other chloride-coupled transport that raises cell chloride above equilibrium, coupled with volume-activated permeabilities, is a possible mechanism of volume regulation. To our knowledge, however, there is no experimental evidence to support the blockage of cell volume regulation in toad bladder or frog skin upon application of stilbene derivatives. In fact, blockage of volume regulation in frog skin after application of furosemide (Ussing, 1982) implies that Na:K:Cl cotransport is the prominent mechanism accounting for increased intracellular chloride. In our study we also considered a voltage-gated Cl channel that would activate upon depolarization of the basolateral membrane. As the basolateral membrane is composed primarily of a K conductance in the steady state, dilution of cell K would depolarize the basolateral membrane. This scheme is viable only if serosal K concentration is left unchanged with the hypotonic shock. In our simulated experiment, however, as well as that of MacRobbie and Ussing (1961), the basolateral Nernst potential E_K remains constant as both serosal and intracellular K are diluted proportionately. Thus, the voltage-gated Cl channel cannot explain volume regulation in our model.

Future studies of the relationship between volume perturbation and ion channel modifications will help elucidate the mechanisms of volume regulation. In particular, it is necessary to measure the K and Cl permeabilities separately to differentiate between their activation properties. The volume regulatory scheme investigated in this paper applies to tight epithelia with high resting basolateral K conductance, so that increases in the rate-limiting Cl permeability will permit the extrusion of K with accompanying Cl during VRD. In such epithelia, the model predicts that although barium would inhibit cell volume regulation by reducing the resting K conductance, blocking the activation of the K permeability above its resting value will not inhibit cell volume regulation. In contrast, the model suggests that activation of Cl channels is essential for volume regulation. In particular, the existence of stretch-activated Cl channels in the basolateral membrane of the toad bladder is a critical test of this model. Although the role of K channels in volume regulatory mechanisms has often been stressed, our model predicts that activation of K channels above a high resting

conductance is unnecessary for volume regulation and that Cl channel activation determines the volume regulatory capacity of the toad bladder and frog skin epithelia.

This investigation was supported by Public Health Service grants 5-R01-DK-31550 (to J. L. Stephenson), 1-R01-DK-29857 (to A. M. Weinstein), and DK-27847 (to L. G. Palmer) from the National Institute of Diabetes and Digestive and Kidney Diseases.

Original version received 12 May 1989 and accepted version received 12 March 1990.

REFERENCES

Cala, P. M. 1980. Volume regulation by Amphiuma red blood cells. The membrane potential and its implications regarding the nature of the ion-flux pathways. *Journal of General Physiology.* 76:683–708.

Chang, D., and D. C. Dawson. 1988. Digitonin-permeabilized colonic cell layers. Demonstration of calcium-activated K and Cl conductances. *Journal of General Physiology.* 92:281–306.

Chase, H. S., and S. Wong. 1985. Cell swelling increases intracellular calcium, a requirement for the increase of K permeability which underlies cell volume regulation. *Kidney International.* 27:305. (Abstr.)

Civan, M. M., and R. J. Bookman. 1982. Transepithelial Na transport and the intracellular fluids: a computer study. *Journal of Membrane Biology.* 65:63–80.

Civan, M. M., T. A. Hall, and B. L. Gupta. 1980. Microprobe study of toad urinary bladder in absence of serosal K. *Journal of Membrane Biology.* 55:187–202.

Davis, C. W., and A. L. Finn. 1982. Sodium transport inhibition by amiloride reduces basolateral membrane potassium conductance in tight epithelia. *Science.* 216:525–527.

Davis, C. W., and A. L. Finn. 1987. Interactions of sodium transport, cell volume, and calcium in frog urinary bladder. *Journal of General Physiology.* 89:687–702.

DiBona, D. R. 1978. Direct visualization of epithelial morphology in the living amphibian urinary bladder. *Journal of Membrane Biology.* Special Issue: 45–70.

Ferreira, K. T. G., and H. G. Ferreira. 1981. The regulation of volume and ion composition in frog skin. *Biochimica et Biophysica Acta.* 646:193–202.

Ferreira, H. G., and K. T. G. Ferreira. 1983. Epithelial transport parameters: an analysis of experimental strategies. *Proceedings of the Royal Society of London B.* 218:309–329.

Finn, A. L., and L. Reuss, 1975. Effects of changes in the composition of the serosal solution on the electrical properties of the toad urinary bladder epithelium. *Journal of Physiology.* 250:541–558.

Garay, R. P., and P. J. Garrahan. 1973. The interaction of sodium and potassium with the sodium pump in red cells. *Journal of Physiology.* 231:297–325.

Geck, P., and E. Heinz. 1980. Coupling of ion flows in cell suspension systems. *Annals of the New York Academy of Sciences.* 341:57–62.

Geck, P., C. Pietrzyk, B.-C. Burckhardt, B. Pfeiffer, and E. Heinz. 1980. Electrically silent cotransport of Na, K, Cl in Ehrlich cells. *Biochimica et Biophysica Acta.* 600:432–447.

Germann, W. J., S. A. Ernst, and D. Dawson. 1986. Resting and osmotically induced basolateral K conductances in turtle colon. *Journal of General Physiology.* 88:253–274.

Giraldez, F., and K. T. G. Ferreira. 1984. Intracellular chloride activity and membrane potential in stripped frog skin (Rana temporaria). *Biochimica et Biophysica Acta.* 769:625–628.

Goldman, D. E. 1943. Potential, impedance, and rectification in membranes. *Journal of General Physiology.* 23:37–60.

Greger, R., E. Schlatter, and F. Lang. 1983. Evidence for electroneutral sodium chloride cotransport in the cortical thick ascending limb of Henle's loop of rabbit kidney. *Pflügers Archiv.* 396:308–314.

Grinstein, S., A. Rothstein, B. Sarkadi, and E. W. Gelfand. 1984. Responses of lymphocytes to anisotonic media: volume-regulating behavior. *American Journal of Physiology.* 246:C204–C215.

Hays, R. M., and A. Leaf. 1962. Studies on the movement of water through the isolated toad bladder and its modification by vasopressin. *Journal of General Physiology.* 45:905–919.

Hoffman, J., and D. C. Tosteson. 1971. Active sodium and potassium transport in high potassium and low potassium sheep red cells. *Journal of General Physiology.* 58:438–466.

Hoffmann, E. K., I. H. Lambert, and L. O. Simonsen. 1986. Separate Ca-activated K and Cl transport pathways in Ehrlich ascites tumor cells. *Journal of Membrane Biology.* 91:227–244.

Hoffmann, E. K., and L. O. Simonsen. 1989. Membrane mechanisms in volume and pH regulation in vertebrate cells. *Physiological Reviews.* 69:315–382.

Hudson, R. L., and S. G. Schultz. 1988. Sodium-coupled glycine uptake by Ehrlich ascites tumor cells results in an increase in cell volume and plasma membrane channel activities. *Proceedings of the National Academy of Sciences.* 85:279–283.

Huss, R. E., and D. J. Marsh. 1975. A model of NaCl and water flow through paracellular pathways of renal proximal tubule. *Journal of Membrane Biology.* 23:305–347.

Hviid Larsen, E. 1978. Computed steady-state ion concentrations and volume of epithelial cells: dependence on transcellular Na transport. *Alfred Benzon Symposium.* 11:438–456.

Hviid Larsen, E., and L. Kristensen. 1978. Properties of a conductive cellular chloride pathway in the skin of the toad (Bufo bufo). *Acta Physiologica Scandinavica.* 102:1–21.

Kirk, K., D. DiBona, and J. Schafer. 1987. Regulatory volume decrease in perfused proximal nephron: evidence for a dumping of cell K. *American Journal of Physiology.* 252:F933–F942.

Koefoed-Johnsen, V., and H. H. Ussing. 1958. The nature of the frog skin potential. *Acta Physiologica Scandinavica.* 42:298–308.

Koenig, B., S. Ricapito, and R. Kinne. 1983. Chloride transport in the thick ascending limb of Henle's loop: potassium dependence and stoichiometry of the NaCl cotransport system in plasma membrane vesicles. *Pflügers Archiv.* 399:173–179.

Kregenow, F. M. 1971*a*. The response of duck erythrocytes to non-hemolytic hypotonic media. *Journal of General Physiology.* 58:372–395.

Kregenow, F. M. 1971*b*. The response of duck erythrocytes to hypertonic media. *Journal of General Physiology.* 58:396–412.

Kregenow, F. M. 1981. Osmoregulatory salt transporting mechanisms: control of cell volume in anisotonic media. *Annual Review of Physiology.* 43:493–505.

Lau, K. R., R. L. Hudson, and S. G. Schultz. 1984. Cell swelling induces a barium-inhibitable potassium conductance in the basolateral membrane of *Necturus* small intestine. *Proceedings of the National Academy of Sciences.* 81:3591–3594.

Levine, S. D., M. Jacoby, and A. Finkelstein. 1984. The water permeability of toad urinary bladder. I. Permeability of barriers in series with the luminal membrane. *Journal of General Physiology.* 83:529–541.

Lew, V. L., H. G. Ferreira, and T. Moura. 1979. The behaviour of transporting epithelial cells: I. Computer analysis of a basic model. *Proceedings of the Royal Society of London B.* 206:53–83.

Lewis, S. A., A. G. Butt, M. J. Bowler, J. P. Leader, and A. D. C. Macknight. 1985. Effects of anions on cellular volume and transepithelial Na transport across toad urinary bladder. *Journal of Membrane Biology.* 83:119–137.

Lopes, A., and W. Guggino. 1987. Volume regulation in early proximal tubule of the *Necturus* kidney. *Journal of Membrane Biology.* 97:117–125.

Macknight, A. D. C. 1985. The role of anions in cellular volume regulation. *Pflügers Archiv.* 405:S12–S16.

Macknight, A. D. C., D. R. DiBona, A. Leaf, and M. M. Civan . 1971. Measurement of the composition of epithelial cells from the toad urinary bladder. *Journal of Membrane Biology.* 6:108–126.

Macknight, A. D. C., D. R. DiBona, and A. Leaf. 1980. Sodium transport across toad urinary bladder: a model "tight" epithelium. *Physiological Reviews.* 60:615–715.

MacRobbie, E. A. C., and H. H. Ussing. 1961. Osmotic behavior of the epithelial cells of frog skin. *Acta Physiologica Scandinavica.* 53:348–365.

Mintz, E., S. R. Thomas, and D. C. Mikulecky. 1986. Exploration of apical sodium transport mechanisms in an epithelial model by network thermodynamic simulation of the effect of mucosal sodium depletion: I. Comparison of three different apical sodium permeability expressions. *Journal of Theoretical Biology.* 123:1–19.

Nagel, W., J. F. Garcia-Diaz, and W. McD. Armstrong. 1981. Intracellular ionic activities in frog skin. *Journal of Membrane Biology.* 61:127–134.

Nielsen, R. A. 1979. 3 to 2 coupling of the Na-K pump responsible for the transepithelial Na transport in frog skin disclosed by the effect of barium. *Acta Physiologica Scandinavica.* 107:189–191.

Oberleithner, H. W., W. Guggino, and G. Giebisch. 1983. The effect of furosemide on luminal sodium, chloride, and potassium transport in the early distal tubule of Amphiuma kidney. *Pflügers Archiv.* 396:27–33.

Rick, R., A. Dörge, E. von Arnim, and K. Thurau. 1978a. Electron microprobe analysis of frog skin epithelium: evidence for a syncytial Na transport compartment. *Journal of Membrane Biology.* 39:313–331.

Rick, R., A. Dörge, A. D. C. Macknight, A. Leaf, and K. Thurau. 1978b. Electron microprobe analysis of the different epithelial cells of toad urinary bladder. *Journal of Membrane Biology.* 39:257–271.

Sackin, H. 1987. Stretch-activated potassium channels in renal proximal tubule. *American Journal of Physiology.* 253:F1253–F1262.

Sackin, H. 1989. A stretch-activated K channel sensitive to cell volume. *Proceedings of the National Academy of Sciences.* 86:1731–1735.

Sands, J. M., M. A. Knepper, and K. R. Spring. 1986. Na-K-Cl cotransport in apical membrane of rabbit renal papillary surface epithelium. *American Journal of Physiology.* 251:F475–F484.

Schultz, S. G. 1981. Homocellular regulatory mechanisms in sodium-transporting epithelia: avoidance of extinction by "flush-through". *American Journal of Physiology.* 241:F579–F590.

Stephenson, J. L. 1978. Analysis of the transient behavior of kidney models. *Bulletin of Mathematical Biology.* 40:211–221.

Strieter, J., J. L. Stephenson, L. G. Palmer, and A. M. Weinstein. 1987. Homeostatic effects of Na:K:Cl cotransport in a mathematical model of toad urinary bladder. *Biophysical Journal.* 51:340*a.* (Abstr.)

Turner, R. J. 1983. Quantitative studies of cotransport systems: models and vesicles. *Journal of Membrane Biology.* 76:1–15.

Ubl, J., H. Murer, and H.-A. Kolb. 1988. Ion channels activated by osmotic and mechanical stress in membranes of opossum kidney cells. *Journal of Membrane Biology.* 104:223–232.

Ussing, H. H. 1982. Volume regulation of frog skin epithelium. *Acta Physiologica Scandinavica.* 114:363–369.

Ussing, H. H. 1985. Volume regulation and basolateral co-transport of sodium, potassium, and chloride ions in frog skin epithelium. *Pflügers Archiv.* 405(Suppl 1):S2–S7.

Ussing, H. H., and E. E. Windhager, 1964. Nature of shunt path and active sodium transport through frog skin epithelium. *Acta Physiologica Scandinavica.* 61:484–504.

Ussing, H. H., and K. Zerahn. 1951. Active transport of sodium as the source of electric current in the short-circuited isolated frog skin. *Acta Physiologica Scandinavica.* 23:110–127.

Weinstein, A. M., and J. L. Stephenson. 1979. Electrolyte transport across a simple epithelium. Steady-state and transient analysis. *Biophysical Journal.* 27:165–186.

Welling, P. A., and M. A. Linshaw. 1988. Importance of anion in hypotonic volume regulation of rabbit proximal straight tubule. *American Journal of Physiology.* 255:F853–F860.

Welling, P. A., and R. G. O'Neil. 1990. Cell swelling activates basolateral membrane Cl and K conductances in rabbit proximal tubule. *American Journal of Physiology.* 258:F951–F962.

Wong, S., and H. Chase. 1986. Role of intracellular calcium in cellular volume regulation. *American Journal of Physiology.* 250:C841–C852.